MRS Advances © 2019 Materials Research Society DOI: 10.1557/adv.2019.437



# Chemical Vapor Growth of Silicon Phosphide Nanostructures

Zhuoqun Wen<sup>#</sup>, Yiping Wang<sup>#</sup>, Zhizhong Chen, Jian Shi<sup>\*</sup>

Department of Materials Science and Engineering, Rensselaer Polytechnic Institute, Troy, NY, 12180

<sup>#</sup>equally contributed

\*correspondence: shij4@rpi.edu

ABSTRACT

In the search for chemically stable two-dimensional (2D) materials with high in-plane mobility, proper bandgap, and compatibility with vapor-based fabrication, van der Waals semiconductor SiP has become a potential candidate as a robust variation of black phosphorous. While bulk SiP crystals were synthesized in the 1970s, the vapor-based synthesis of SiP nanostructures or thin films is still absent. We here report the first chemical vapor growth of SiP nanostructures on SiO<sub>2</sub>/Si substrate. SiP islands with lateral size up to 20 µm and showing well-defined Raman signals were grown on SiO<sub>2</sub>/Si substrate or on SiP-containing concentric rings. The presence of SiP phase is confirmed by XRD. The formation of rings and islands is explained by a multiple coffee ring growth model where a dynamic fluctuation of droplet growth front induces the topography of concentric ring surfaces. This new growth method might shed light on the controlled growth of group IV-III high-mobility 2D semiconductors.

### INTRODUCTION

Two dimensional (2D) materials with high in-plane charge carrier mobility, proper bandgap, sufficient chemical stability, and compatibility with vapor-based fabrication methods are highly desired in the semiconductor community. Graphene has high room-temperature mobility > 10000 cm<sup>2</sup>/V•s but zero bandgap [1]. Transition metal dichalcogenides (TMDCs) have bandgap 1.0 eV~1.9 eV while carrier mobility is

typically below 200 cm²/V•s due to the presence of transition metals [2, 3]. Among 2D semiconductors composed of main-group elements, black phosphorus (BP) has ideal room-temperature mobility ~400 cm²/V•s and bandgap ~2 eV [4]. However, BP family is vulnerable under ambient environment [5]. Although BP and its derivatives can be stabilized by alloying with group V elements without compromising mobility and bandgap much, e.g. AsP [5], their vapor-based synthesis has so far remained challenging.

Inspired by the alloying of BP, 2D van der Waals (vdW) semiconductor SiP, a chemically-stabilized variant of BP, re-evoked the attention of semiconductor research in recent years [6]. As shown in figure 1(a), the room temperature phase of SiP has an orthorhombic structure with space group Cmc21 [7]. Each layer is composed of wurtzitelike interconnected tetrahedral sites that compose both Si-P and Si-Si bonds. Between neighbouring layers, a vdW gap ~2.9 Å is opened between bonded P atoms to sustain local charge neutrality. Qualitatively, the decent electronic properties of SiP can be understood from two aspects. On the one hand, the unique Si-like vdW structure resembles the sp3 hybridization of Si tetrahedron and in turn inherits its high carrier mobility. On the other hand, the presence of P not only induces a larger yet near direct bandgap compared to Si, but also opens up a vdW gap. Based on DFT calculations, SiP shows a near direct bandgap of 1.69 eV with CBM and VBM located at  $\Gamma$  and S $\rightarrow$ Y, respectively. The calculated band edges turn out rather dispersive, indicating a potential for high carrier mobility [8]. Back to the 1970s, bulk crystals of SiP and other groups IV-III compounds SiP2, SiAs, and GeAs were synthesized by chemical vapor transport (CVT) or high-pressure melt growth [9, 10], while the vapor-based synthesis of SiP single crystalline flakes or nanosheets remains unexplored.

In this work, we demonstrate the vapor-based growth of SiP nanostructures for the first time. Using a unique transport-agent-assisted chemical vapor deposition, SiP rings with diameters up to  $\sim 100~\mu m$  and islands with lateral size up to  $\sim 5~\mu m$  were grown on SiO<sub>2</sub>/Si substrate. The crystal structure was confirmed by XRD and Raman spectroscopy. Different kinds of ring or island structures exhibited rather distinctive Raman signals and could be well explained by the "multiple coffee ring" growth model we proposed.

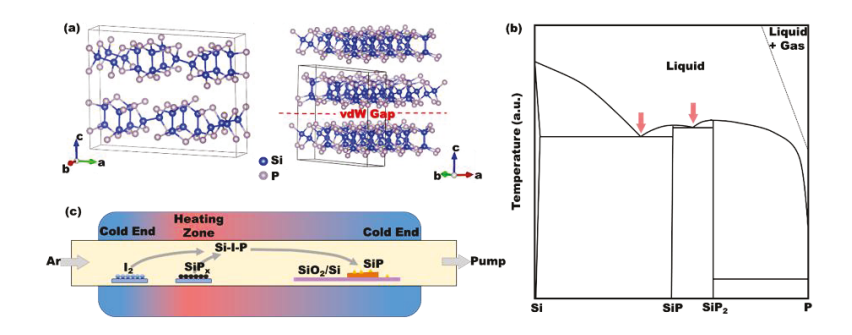


Figure 1. (a) Ball-stick model of SiP, showing a mixture of Si-Si and Si-P bonds, and the interlayer van der Waals gap. The unit cell is defined by the black straight lines [7]. (b) The Si-P binary phase diagram, where the two eutectic points ~1100 °C are marked by two downward red arrows [11]. (b) is adapted and reprinted with permission from Springer Nature. (c) Design of transport-agent-assisted chemical vapor deposition of SiP.

## **EXPERIMENTAL DETAILS**

Back to the 1970s, I<sub>2</sub>, Br<sub>2</sub>, or Cl<sub>2</sub> were used as transport agent in CVT of bulk [9, 12, 13]. Typically, following reactions GeAs  $2SiAs(s)+7I_2 \rightleftharpoons 2SiI_4(g)+2AsI_3(g)$  or  $GeAs(s)+2I_2(g) \rightleftharpoons GeI_4(g)+As(s)$ . The species were transported between a hot end around 1100~1200 °C and a cold end around 600 °C over a few days [12]. As shown in figure 1(b), the Si-P binary system is featured by two eutectic transitions near 1100 °C, while the P-rich region shows a much lower transition temperature ~600 °C [11]. We also notice that the CVT reaction between SiP<sub>2</sub> and I<sub>2</sub> will further facilitate the transport process [9]. Therefore, with the aid of excess P and I<sub>2</sub> in the vapor phase, the precipitation temperature of Si-P compounds (hereafter referred to as SiP<sub>x</sub>) could be lowered significantly so that vapor-based growth of SiP<sub>x</sub> could probably be achieved in a conventional chemical vapor deposition (CVD). We therefore resorted to a transport-agent-assisted CVD to deposit SiP on SiO<sub>2</sub>/Si substrates in a horizontal tube furnace. As sketched in figure 1(c), SiP<sub>x</sub> powder was prepared by ball milling Si and red-P and used as starting precursors and loaded in a heating zone center; I<sub>2</sub> were placed in the upper stream area while SiO<sub>2</sub>/Si substrates were placed to the downstream area. In a typical growth cycle, high-purity Ar was flown at a rate of 100 sccm through the whole growth process and the pressure inside the tube was maintained at ~200 Torr. The zone center was ramped to 1100°C within 3 h and dwelled at 1100 °C overnight, after which the furnace was cooled down naturally to room temperature. The positions of  $I_2$  and  $SiO_2/Si$  were chosen, such that  $I_2$  were heated to ~100 °C to sustain a constant supply of I<sub>2</sub> vapor, while substrate temperature was around 800 °C to enhance SiP crystallinity.

## RESULTS

The morphologies of as-grown SiP structures (whose phase was identified later) are shown in figure 2. Based on the optical image in figure 2(a), SiP were formed as colonies of concentric rings with the largest radius ~80  $\mu m$ . The homogeneous blue/green color (partially induced by the purple background of SiO2/Si substrate) of ring structures and the lack of defocus in optical image indicate that the height variation over these colonies is small. As the colonies expand and touch each other, polyhedron domains were formed. In addition to rings, brown islands with lateral size ~2  $\mu m$  were formed atop of rings or near the domain boundaries where rings were absent.

The AFM image of a typical colony is shown in figure 2(b). The height of the colony ranged between  $700{\sim}800$  nm, whose small variation is consistent with optical images. The width of individual rings increased from <1  $\mu$ m to ~5  $\mu$ m deviating away from the ring center. Between neighboring rings, a groove is formed, whose depth is <5% of the height of the rings. We also noticed that the top surfaces of rings are fluctuating. Compared to the layer-by-layer growth of 2D materials where a locally smooth, groove-free terrace structure is formed, the locally rough concentric rings separated by grooves observed in SiP is rather distinctive.

Figure 2(c)(d)(e) show the SEM images of SiP rings. The densely arranged rings shown in figure 2(e) were taken near the ring center. The grooves and local height deviation were clearly observed. For the sake of analysis, we hereafter refer to the four kinds of morphologies as off-center rings, central rings, on-ring islands, off-ring islands, figure 2(c).

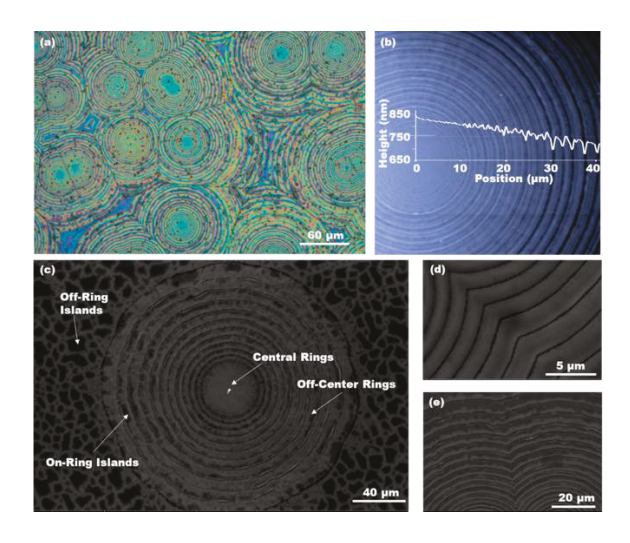


Figure 2. Growth results of SiP. (a) Optical image of SiP grown on SiO<sub>2</sub>/Si. (b) AFM imagine of a typical SiP colony. The height profile was traced along the horizontal axis. (c) Global view of a typical colony where four kinds of morphologies are designated. (d)(e) Closer view of grooves and narrow rings.

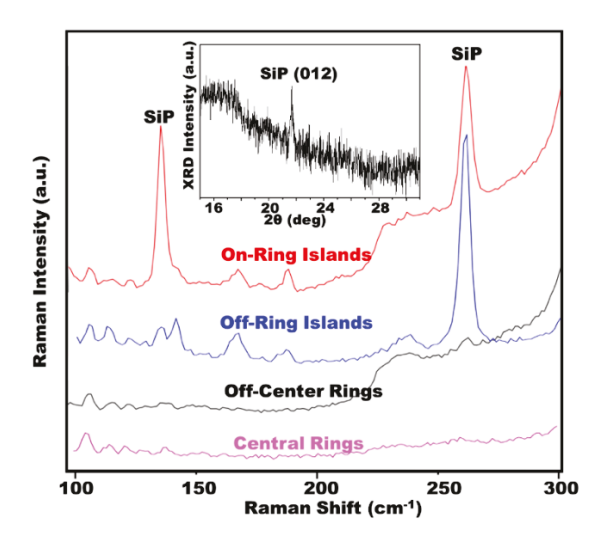


Figure 3. Raman spectra of off-center rings, central rings, on-ring islands and off-ring islands. The two characteristic peaks of SiP are indexed. The inset shows the XRD pattern of the sample where the SiP (012) peak is identified.

Figure 3 shows the Raman spectroscopy spectra and XRD pattern of SiP. The (120) peak at  $20\sim22^\circ$  is consistent with bulk crystals [7]. There are not any other XRD peaks beyond the range of  $2\theta$  at  $15^\circ\sim30^\circ$ . The low XRD intensity in our case may be caused by the low coverage of SiP on SiO<sub>2</sub>/Si substrate. However, SiP phase can still be identified based on Raman spectroscopy and XRD. The Raman spectra from the four different morphologies are compared in figure 3. The on-ring islands showed two duplicated sharp Raman peaks near 131 cm<sup>-1</sup> and 262 cm<sup>-1</sup>, consistent with previous reports on SiP [14]. The 131 cm<sup>-1</sup> peak was absent among off-ring islands. In addition,

some tiny peaks between 100~200 cm<sup>-1</sup> were observed from on-ring islands or off-ring islands. Indexation of Raman modes of SiP is still unknown at present [14]. The shoulder-like peak starting from 225 cm<sup>-1</sup> was attributed to SiO<sub>2</sub>/Si. In contrast, rather weak Raman signals were observed from both kinds of rings. Therefore, the crystallinity of different SiP structures may be ranked as on-ring islands>off-ring islands>off-center rings>central rings. It should be noted that the low-crystallinity structures might not contribute to XRD signal much.

#### DISCUSSIONS

The growth process of SiP and how it further influences the crystallinity of different structures can be explained with a multiple coffee ring growth model. The multiple coffee ring structure has been observed in the evaporation of colloidal droplet on a flat substrate [15-18]. The fact that the surface curvature of a cap-shaped droplet is larger near the periphery than near the center will accelerate the evaporation of liquid near droplet periphery (e.g. Gibbs-Thomson Effect) [19]. Based on mass conservation, the solution near the droplet center must flow towards the periphery to replenish the higher evaporation rate therein [15]. Due to the interaction among capillary flow, surface tension, and viscosity, the droplet periphery can be temporarily pinned by tiny features on the substrate surface or by the newly precipitated solute at the periphery (i.e. the growth front), rendering the eccentric capillary flow more significant [16-18].

Near periphery, the height-averaged radial velocity of solution with a distance r from the droplet center can be quantified as equation 1 [18],

$$u(r,t) = \frac{D}{\theta(t)\sqrt{R(R-r)}}\#(1)$$

Where D represents the driving force of the flow, R the droplet radius,  $\theta(t)$  the contact angle. The  $[R(R-r)]^{-1/2}$  dependence is due to the aforementioned diverging evaporation rate at the droplet surface. When the growth front is pinned,  $\theta(t)$  keeps decreasing due to the steady evaporation of liquid. As a result, u(r,t) in turn increases. Therefore, the precipitation rate and the supersaturation of solute keep scaling up with time, such that an order-to-disorder transition of the precipitated solute is induced with R shrinking.

However, if the evaporation rate is so high that the radial flow of solution can no longer replenish the evaporation, the pinned growth front will have to recede centripetally before  $\theta(t)$  reaches zero [20]. In this way, the reduced R, along with an increased  $\theta(t)$  would allow for a larger u(r,t), so that the evaporation rate can again be balanced by the eccentric solution flow. After reaching  $\theta_{max}$ , the eccentric solution flow outweighs the evaporation rate, the formation of rings becomes difficult, and the pinned growth front breakdowns again. In this regard, when the overall evaporation is rather high (compared to near-room-temperature evaporation of colloidal suspensions etc.), a droplet would undergo a dynamic yet repeated "pin-unpin-pin-unpin..." cycle instead of a monotonic exhaustion with only one pinned growth front; and accordingly a colony of multiple rings with fluctuating surface topography rather than one single ring is expected.

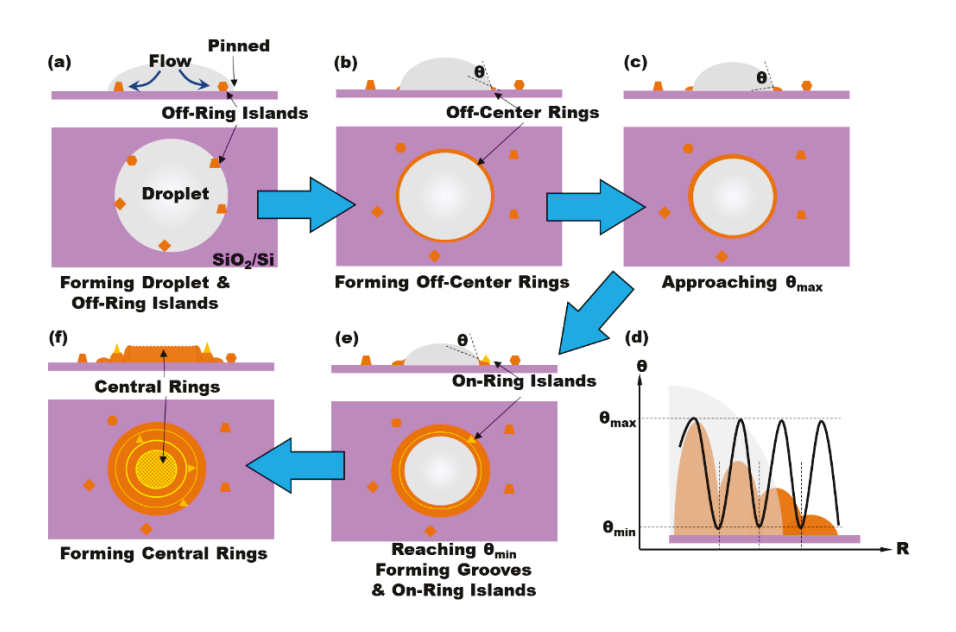


Figure 4. The proposed multiple coffee ring growth mode of SiP. (a) After the droplet is formed and its periphery pinned, eccentric flow of solution inside the droplet starts, eventually off-ring islands are precipitated. (b) Off-center rings are formed with droplet radius shrinking. (c) When the contact line is unpinned, contact angle  $\theta$  gradually increases. (d) The fluctuation of contact angle  $\theta$  as a function of droplet radius R. The topography of rings' colony is plotted, showing that the minimum contact angle  $\theta_{min}$  coincides with the grooves. (e) When the minimum contact angle is reached, a groove is formed. On-ring islands are grown from vapor phase. (f) The central rings are formed at the final stage of evaporation.

In the vapor-phase growth of SiP, the higher reaction rates and larger supersaturation will induce more off-equilibrium growth than colloid evaporation. As sketched in figure 4(a), the pinned growth front will induce a low local Si concentration, and give rise to SiP crystals inside the droplet, i.e. off-ring islands. It should be noted that these off-ring islands are formed under (near) equilibrium growth condition. With evaporation proceeds, the periphery recedes centripetally, leaving the off-ring islands exposed. In the next stage, figure 4(b), the droplet will undergo the aforementioned order-to-disorder transition such that off-center rings formed under off-equilibrium condition are precipitated at growth front. It should be noted that the exact composition of off-center rings or central rings cannot be identified since no characteristic Raman signal could be detected. The dynamic pin-unpin-pin cycles are depicted in figure 4(c)(d)(e). With R decreasing, the contact angle starts to increase from  $\theta_{min}$  right after unpinning. The oscillation of  $\theta$  corresponds to the topography of rings, as sketched in figure 4(d), where the grooves correspond to  $\theta_{min}$ . It should be noted that the height fluctuation we observed is <5% of the overall height of these rings, in stark contrast with conventional coffee ring structures where neighbouring rings are separated. The close distribution in our case can be explained by the much faster precipitation of solutes compared to the case of colloids. Meanwhile, adatoms like Si-P-I will deposit atop of the rings and grow into on-ring islands. It should be noted that on-ring islands may be grown from vapor phase via homogeneous nucleation, rendering them rather high crystallinity. Chances that islands are directly grown from vapor phase onto bare substrate via heterogeneous nucleation are non-negligible though much smaller compared to the formation of on-ring islands. In the final stage sketched in figure 4(f), a collection of densely-arranged central rings are formed. When the droplet diameter is small and comparable with the droplet height, the surface tension effect becomes rather significant such that the evaporation rate at growth front fluctuates more frequently. This qualitative picture might explain the smaller intervals between adjacent central rings compared to off-center rings, and the lower crystallinity of central rings compare to off-center rings. Based on the growth process proposed above, the crystallinity of the four kinds of SiP structures can be ranked as on-ring islands > off-ring islands > off-center rings > central rings, consistent with the observation of Raman spectroscopy.

#### CONCLUSIONS

The "islands plus rings" nanostructure of two-dimensional vdW semiconductor SiP was grown by I<sub>2</sub>-assisted chemical vapor deposition on SiO<sub>2</sub>/Si substrates for the first time. The presence of SiP phase was confirmed by Raman spectroscopy and XRD. Concentric rings with the utmost diameter around 80 µm showed up as closelydistributed colonies. With approaching the ring center, the interval between adjacent rings decreased from  $\sim$ 5 µm to <1 µm, while the height increased from  $\sim$ 700 nm to  $\sim$ 800 nm. Some 5~20 µm large islands were formed near the boundaries of neighboring colonies of concentric rings, while some <5 µm islands were grown atop of concentric rings. The two kinds of islands show strong Raman signals similar to bulk crystals. The formation of "multiple coffee rings" compared to the well-known single coffee ring growth mode in colloidal systems was explained by a dynamic pin-unpin-pin cycle of the droplet growth front. The formation of islands and rings and their different crystallinities were explained with multiple coffee ring growth model. Up to our knowledge, this is the first demonstration of the vapor-based growth of SiP nanostructures. The innovative growth method may shed light on the controlled growth of SiP or similar group IV-III compounds, and eventually pave the road for the exploration of new stable, highmobility two-dimensional semiconductors.

# ACKNOWLEDGMENTS

J.S. was supported by the NYSTAR Focus Center (award number C150117). J.S. and Y.W. were supported by the AFOSR under award number FA9550-18-1-0116. Z.C. and Z.W. were supported by the USA National Science Foundation under award number 1706815.

## **REFERENCES**

- K. I. Bolotin, K. J. Sikes, Z. Jiang, M. Klima, G. Fudenberg, J. Hone, P. Kim and H. L. Stormer, Solid State Commun. 146 (9), 351-355 (2008)
- M. Chhowalla, H. S. Shin, G. Eda, L.-J. Li, K. P. Loh and H. Zhang, Nat. Chem. 5, 263 (2013).
- B. Radisavljevic, A. Radenovic, J. Brivio, V. Giacometti and A. Kis, Nat. Nanotechnol. 6 (3), 147-150 (2011).
- F. Xia, H. Wang and Y. Jia, Nat. Commun. 5 (1), 4458 (2014).
- B. Liu, M. Köpf, A. N. Abbas, X. Wang, Q. Guo, Y. Jia, F. Xia, R. Weihrich, F. Bachhuber, F. Pielnhofer, H. Wang, R. Dhall, S. B. Cronin, M. Ge, X. Fang, T. Nilges and C. Zhou, J. Adv. Mater. 27 (30), 4423-4429 (2015).
- B. Huang, H. L. Zhuang, M. Yoon, B. G. Sumpter and S.-H. Wei, Phy. Rev. B 91 (12), 121401 (2015).
- C. Li, S. Wang, X. Zhang, N. Jia, T. Yu, M. Zhu, D. Liu and X. Tao, CrystEngComm 19 (46), 6986-6991 (2017).
- S. Zhang, G. Shiying, Y. Huang, Z. Zhu, B. Cai, M. Q. Xie, W. Zhou and H. Zeng, 2D Mater. 4, 015030 (2016).
- 9. P. C. Donohue, W. J. Siemons and J. L. Gillson, J. Phys. Chem. Solids **29** (5), 807-813 (1968).
- M. Binnewies, R. Glaum, M. Schmidt and P. Schmidt, in *Chemical vapor transport reactions* (Walter De Gruyter Publisher, Berlin; Boston, 2012), p. 460.
- 11. S.-M. Liang and R. Schmid-Fetzer, J. Phase Equilib. Diff. 35 (1), 24-35 (2014).
- R. Hillel, C. Bec, J. Bouix, A. Michaelides, Y. Monteil, A. Tranquard and C. Bernard, J. Electrochem. Soc. 129 (6), 1343-1347 (1982).
- 13. R. Hillel, J. Bouix and A. Michaélidès, Thermochim. Acta 38 (3), 259-269 (1980).
- 14. C. Barreteau, B. Michon, C. Besnard and E. Giannini, J. Cryst. Growth 443, 75-80 (2016).
- R. D. Deegan, O. Bakajin, T. F. Dupont, G. Huber, S. R. Nagel and T. A. Witten, Nature 389 (6653), 827-829 (1997).
- 16. R. H. Dettre and R. E. Johnson, in *Contact Angle, Wettability, and Adhesion* (American Chemical Society, 1964), Vol. 43, pp. 136-144.
- 17. B. J. Fischer, Langmuir **18** (1), 60-67 (2002).
- Á. G. Marín, H. Gelderblom, D. Lohse and J. H. Snoeijer, Phy. Rev. Lett. 107 (8), 085502 (2011).
- 19. D. A. Porter, K. E. Easterling and M. Sherif, *Phase Transformations in Metals and Alloys* (CRC press, 2009) p. 44.
- X. Shen, C.-M. Ho and T.-S. Wong, J. Phys. Chem. B 114 (16), 5269-5274 (2010).